

Analytical model for Rayleigh-Taylor instabilityin conical target conduction region

Zhong-Yuan Zhu(朱仲源), Yun-Xing Liu(刘云星), Ying-Jun Li(李英骏), and Jie Zhang(张杰)
Citation: Chin. Phys. B, 2022, 31 (**10**): 105202. DOI: 10.1088/1674-1056/ac8731
Journal homepage: http://cpb.iphy.ac.cn; http://iopscience.iop.org/cpb

What follows is a list of articles you may be interested in

Scaling of rise time of drive current on development of magneto-Rayleigh-Taylor instabilities for single-shell Z-pinches

Xiaoguang Wang(王小光), Guanqiong Wang(王冠琼), Shunkai Sun(孙顺凯), Delong Xiao(肖德龙), Ning Ding(丁宁), Chongyang Mao(毛重阳), and Xiaojian Shu(束小建)
Chin. Phys. B, 2022, 31 (**2**): 025203. DOI: 10.1088/1674-1056/ac1fd9

Weakly nonlinear multi-mode Bell–Plesset growth in cylindrical geometry

Hong-Yu Guo(郭宏宇), Tao Cheng(程涛), and Ying-Jun Li(李英骏)
Chin. Phys. B, 2020, 29 (**11**): 115202. DOI: 10.1088/1674-1056/ab9c14

Numerical study on magneto-Rayleigh-Taylor instabilities for thin liner implosions on the primary test stand facility

Xiao-Guang Wang(王小光), Shun-Kai Sun(孙顺凯), De-Long Xiao(肖德龙), Guan-Qiong Wang(王冠琼), Yang Zhang(张扬), Shao-Tong Zhou(周少彤), Xiao-Dong Ren(任晓东), Qiang Xu(徐强), Xian-Bin Huang(黄显宾), Ning Ding(丁宁), Xiao-Jian Shu(束小建)
Chin. Phys. B, 2019, 28 (**3**): 035201. DOI: 10.1088/1674-1056/28/3/035201

Coupling between velocity and interface perturbations in cylindrical Rayleigh-Taylor instability

Hong-Yu Guo(郭宏宇), Li-Feng Wang(王立锋), Wen-Hua Ye(叶文华), Jun-Feng Wu(吴俊峰), Wei-Yan Zhang(张维岩)
Chin. Phys. B, 2018, 27 (**5**): 055205. DOI: 10.1088/1674-1056/27/5/055205

Rayleigh-Taylor instability at spherical interfaces of incompressible fluids

Hong-Yu Guo(郭宏宇), Li-Feng Wang(王立锋), Wen-Hua Ye(叶文华), Jun-Feng Wu(吴俊峰), Ying-Jun Li(李英骏), Wei-Yan Zhang(张维岩)
Chin. Phys. B, 2018, 27 (**2**): 025206. DOI: 10.1088/1674-1056/27/2/025206

Analytical model for Rayleigh–Taylor instability in conical target conduction region

Zhong-Yuan Zhu(朱仲源)[1], Yun-Xing Liu(刘云星)[2], Ying-Jun Li(李英骏)[1,2,†], and Jie Zhang(张杰)[3]

[1] *School of Science, China University of Mining and Technology, Beijing* 100083, *China*

[2] *Double-cone Ignition (DCI) Joint Team, State Key Laboratory for Geomechanics and Deep Underground Engineering, China University of Mining and Technology, Beijing* 100083, *China*

[3] *Double-cone Ignition(DCI) Joint Team, Beijing National Laboratory for Condensed Matter Physics, Institute of Physics, Chinese Academy of Sciences, Beijing* 100190, *China*

(Received 22 May 2022; revised manuscript received 19 July 2022; accepted manuscript online 5 August 2022)

This work builds an isobaric steady-state fluid analytical-physical model of the plasma conduction region in a conical target. The hydrodynamic instability in the double-cone ignition scheme[21] for inertial confinement fusion (ICF) proposed by Zhang is studied with the built model. With this idealized model, the relevant parameters, such as density, temperature, and length of the plasma in the conduction region of the conical target under long-pulse conditions are given. The solution of the proposed analytical model dovetails with the trend of the numerical simulation. The model and results in this paper are beneficial for discussing how to attenuate Rayleigh–Taylor instability in ICF processes with conical and spherical targets.

Keywords: double-cone ignition, Rayleigh–Taylor instability, conical target conduction region

PACS: 52.57.Fg, 47.20.Ma, 52.35.Py **DOI:** 10.1088/1674-1056/ac8731

1. Introduction

In inertial confinement fusion (ICF)[1–10] schemes with directly driven conical and spherical targets, the Rayleigh–Taylor instability (RTI) imposes a fundamental constraint on the design parameters required for both of these ignition schemes.[11–14] Livescu *et al.*[15–17] studied RTI using direct numerical simulations. Yu and Ye[18] also adopted numerical simulations of hydrodynamic instabilities during direct-drive ICF implosion ignition based on the LARED-S program, but these were for the spherical target. In 1986, a formalism for the semi-analytical form of RTI in spherical geometry was developed by Gupta and Lawand.[19] In 1996, Sanz proposed a self-consistent analytical model for RTI in ICF.[20] Most of the works mentioned above are restricted to numerical simulations or only aim to study RTI in direct-drive spherical targets. In 2020, Zhang proposed a new ignition scheme,[21] i.e., the double-cone ignition scheme (Fig. 1). It is well known that during the direct drive of a spherical target pellet, the ablation front is unstable, affecting the central implosion ignition of the pellet. However, what is actually affected by RTI during laser-irradiated conical targets is the compression process.[22,23] In 2022, Fang and Zhang *et al.*[24] conducted experimental and numerical simulations to study RTI in conical targets caused by factors such as the thickness of the target pellet, but their work ignored the effect of laser-plasma instability (LPI).

Studies have been carried out on the heat conduction region. De Groot[25] proposed an analytical model of a planar plasma in 1992, which explicitly includes the temporal evolution of the heat conduction region. Models for the one-dimensional resolution of the plasma in the conduction region in a planar target have been given by Chang and Li,[26–28] respectively. In 2020, Betti *et al.*[29] also presented a semi-analytical model of the hot spot and compressible shell, using analytical and simulation methods to study the physics of burn propagation in inertially confined plasmas. In Refs. [30–32], the parameters of the heat conduction region in the planar target have also been investigated experimentally[30] and numerically[31,32] by numerous researchers. Notably, in order to better analyze and solve the RTI of the compression process, the authors developed an analytical model of the plasma in the conduction zone instead of modeling the hydrodynamic instability of the ablation surface. Moreover, for the purpose of this paper, the parameters of the plasma (length, density, temperature, etc.) in the conduction zone are given below.

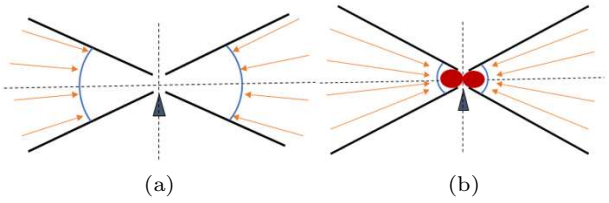


Fig. 1. (a) Schematic of the initial stage. The yellow line in this diagram is the drive laser; the two sides are composed of symmetrical metal walls; and the ignition assembly is placed in the center of the entire unit. (b) Schematic of the compression stage. As the compressed fuel is ejected at high speed and fused together, the ignition assembly ignites and triggers fusion.[33]

The authors ignored the viscosity between the two metal walls and the fusion fuel. The incompressibility (i.e., isobaric approximation) has been widely used in the analytical treatment of the ablation RTI at the ablation front over the past decades. The formula for the growth rate of RTI[34–36] at the

†Corresponding author. E-mail: lyj@aphy.iphy.ac.cn

© 2022 Chinese Physical Society and IOP Publishing Ltd

ablation front in ICF is expressed as follows:

$$\gamma = \sqrt{Akg/(1+AkL)} - \beta k V_a, \tag{1}$$

where k is the perturbed wave number; Atwood number $A = (\rho_2 - \rho_1)/(\rho_2 + \rho_1)$, g is the acceleration; V_a is the ablation velocity; $\beta \approx 2$–4 is expected in the direct-drive ablation; and L is the thickness of the fluid density layer. In combination with the specific parameters of the plasma obtained through the analytical model developed in this paper, it is necessary to analyze the RTI of the compression process in a conical target. This is the reason for and significance of the model described in this paper, and the analytical results are more intuitive than the numerical solutions.

2. Analytical model and application

Since the laser is uniformly irradiated on the spherical target, the polarization angle of the laser irradiation is 2π. However, in the conical target model, the angle becomes smaller compared to that of the former. The authors temporarily define this angle as θ, which ranges from 90° to 120° . Namely, the current study in this paper is two-dimensional (2D).

In Ref. [26], Li gave a one-dimensional self-similar model based on the hydrodynamic behavior of a flat target. Based on research by previous scholars, this paper introduces the physical process of the conduction region in the direct driven conical target model (Fig. 2), focusing on the fluid behavior and properties exhibited by the plasma in the conduction region.

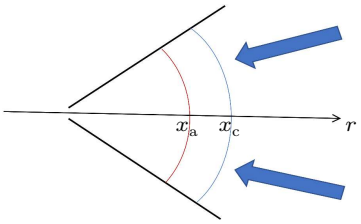


Fig. 2. Diagram of conical target conduction region. The authors define x_a as the ablation surface and x_c as the critical density surface. In addition, x_c is the coordinate origin.

When laser irradiates a solid target to generate plasma, the whole region is usually divided into three regions,[37,38] i.e., the compression region, conduction region and corona region. The boundary between the conduction and corona regions is the critical density surface. The generation of the plasma conduction region of the laser-irradiated conical target consists of three steps. First, the laser acts on the critical density surface of plasma on the conical target, and is absorbed mainly in the corona region since it cannot enter the critical density surface. Plasma heats the conduction region via electron heat conduction. In the 2D case, the electron heat conduction model[39,40] is expressed as

$$Q_r = -\frac{2}{7} k_0 \frac{\partial T_e^{7/2}}{\partial r}, \tag{2}$$

where Q_r is heat flux; T_e is electron temperature; and the heat flux is $Q = -\kappa \partial T_e/\partial r$, where κ is thermal conductivity and $\kappa \propto T_e^{5/2}$. Therefore, the heat energy entering the conduction region through electron heat conduction is the main energy source for plasma generation. Second, the plasma generated by the ablation of the solid material flows away from the ablation surface. The mass of a conical target ablated in unit time is called an ablation rate and is represented by $\mathrm{d}m/\mathrm{d}t$. Third, the authors consider that the driving laser is a long pulse, the conduction region reaches a steady state, and the fluid behavior in the conduction region is steady. The electron heat conduction increases the temperature in the conduction region, while the ablation decreases the temperature and increases the density. The expansion of the plasma results in decreases in its temperature and density. Many factors cause the plasma in the conduction region to expand isobarically. Therefore, the authors adopted an isobaric assumption in this model.

Considering that the authors mainly study the conduction region with electron density $n_e > n_c$ away from the target in space, it is heat conduction, expansion, ablation, and other factors in this region that lead to its equilibrium state. Therefore, plasma fluids can be seen as quasi-steady. As the laser is completely absorbed in the corona region, in the heat conduction region, $T_e \gg T_i$, $P \approx P_e$, and $Q \approx Q_e$ (T_e is the temperature of electrons; T_i is the temperature of ions; P_e is the pressure of electrons; and Q_e is the electronic heat flux). At the same time, assuming that the laser irradiation uniformity is good, the authors consider that the fluid behavior in the conduction region conforms to the steady-state assumption. Then, the expression for the single-fluid, steady-state, and viscous-free hydrodynamic equations are as follows:

$$\frac{\partial \rho}{\partial t} + \frac{\partial(\rho r^2 u)}{r^2 \partial r} + \frac{\partial(\rho v \sin\theta)}{r \sin\theta \partial\theta} = 0, \tag{3}$$

$$\frac{\partial \rho u}{\partial t} + \frac{\partial r^2 \rho u^2}{r^2 \partial r} + \frac{\partial \sin\theta \rho u v}{r \sin\theta \partial\theta} + \frac{\rho v^2}{r} = -\frac{\partial P}{\partial r}, \tag{4}$$

$$\frac{\partial \rho v}{\partial t} + \frac{\partial r^2 \rho u v}{r^2 \partial r} + \frac{\partial \sin\theta \rho v^2}{r \sin\theta \partial\theta} + \frac{\rho v u}{r} = -\frac{1}{r}\frac{\partial P}{\partial \theta}, \tag{5}$$

$$\begin{aligned} &\frac{\partial(\rho E)}{\partial t} + \frac{\partial(\rho E u r^2)}{r^2 \partial r} + \frac{\partial(\rho v E \sin\theta)}{r \sin\theta \partial\theta} \\ &= -P\left[\frac{\partial(r^2 u)}{r^2 \partial r} + \frac{\partial(v \sin\theta)}{r \sin\theta \partial\theta}\right] + \frac{\partial(r^2 Q_r)}{r^2 \partial r} + \frac{\partial(\sin\theta Q_\theta)}{r^2 \sin\theta \partial\theta}, \end{aligned} \tag{6}$$

where ρ, P, and $u(v)$ are the density, pressure, and velocity, respectively, of the plasma; $E = \varepsilon + (u^2/2)$; ε is the internal energy per unit mass; and Q is the heat flux.

In order to facilitate the use of the analysis results of the self-similar equation, the authors adopted convenient units, as shown in Table 1.

Table 1. Normalized values for scaled variables.

Time (t) (s)	Laser intensity (I) (10^{14} W/cm^2)	Wavelength (λ) (μm)	Ionic charge (Z)	Atomic mass (A)	Coulomb logarithm (Λ)
10^{-9}	3	0.351	65	240	5

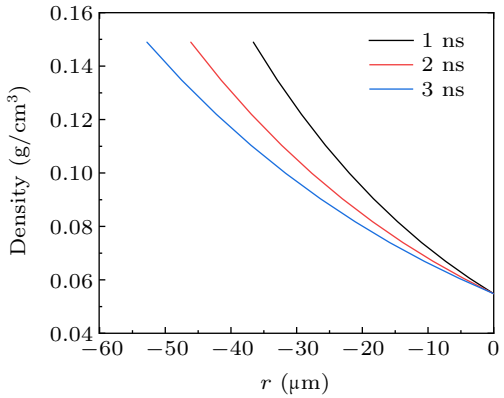


Fig. 3. Evolution of density of plasma as a function of the spatial location for different pulse widths. Laser pulse widths of 1 ns, 2 ns, and 3 ns were randomly selected. Driving laser power density $I = 3.0 \times 10^{14}$ W/cm^2.

Due to Eq. (4) and the ideal gas condition, the authors consider the pressure formula $P = \rho C_s^2$ in Ref. [25], and the pressure in the conduction region is constant at P_c,

$$\frac{\partial P_c}{\partial r} = 0. \tag{7}$$

To define a time-dependent plasma length factor L_r, the formula for the density is

$$\rho(r,t) = c\mathrm{e}^{-r/L_r}. \tag{8}$$

The authors define the critical density surface as the origin of the column coordinates. When $r = 0$, $\rho = \rho_c$, resulting in

$$\rho(r,t) = \rho_c \mathrm{e}^{-r/L_r}, \tag{9}$$

and the mass of ablation is

$$m = \iint \rho(r,t) r \mathrm{d}r\mathrm{d}\theta = \rho_c \theta L_{r\max}^2; \tag{10}$$

therefore, the authors obtain the density description of the conduction zone

$$\rho = \frac{m}{\theta L_{r\max}^2} \mathrm{e}^{-r/L_r}. \tag{11}$$

According to the formula $n_c = (m_e\omega^2/4\pi e^2) \approx 1.1 \times 10^{21}\ \mathrm{cm}^{-3} \cdot \lambda_{\mu\mathrm{m}}^{-2}$ and the relationship between ρ_c and n_c [$\rho_c = (A/N_0 Z) n_c$],[41] the critical surface density is

$$\rho(r,t) = 5.48 \times 10^{-2} Z^{-1} A \mathrm{e}^{-r/L_r}\ \mathrm{g \cdot cm}^{-3}. \tag{12}$$

Solution (11) for the density shows that the length of the plasma and the angle θ of the conical target can affect the changing pattern of the density. When θ is kept constant, the longer the length of the plasma, the slower the density decreases; whereas, when L_r is kept constant, the larger the θ, the steeper the density decrease trend of the plasma in the conduction zone. Figure 3 shows that when the pulse time or laser intensity is properly enhanced, the width of the conduction zone becomes larger and the density of the plasma decreases slowly, which is favorable for reducing the effects caused by RTI.

The pulsed laser energy is absorbed in the corona region and cannot enter the conduction region. According to the work of De Groot *et al.*,[42,43] $\rho u = \mathrm{d}m/\mathrm{d}t$, which is the ablation rate equation. From Eq. (6) and the pressure equation, the authors obtain $C_s^2 \dot{m}(1 + (u^2/2C_s^2)) = -Q_r$. It is known that $E = \varepsilon + (1/2)u^2$ and $\varepsilon = (3/2) m_e C_s^2$, while $m_e = 9.1 \times 10^{-31}$ g, which is so small that it can be ignored. The plasma fluid velocity in the conduction region is less than the velocity of sonic surface, which leads to $0 \le (u^2/C_s^2) \le 1$, resulting in

$$C_s^2 \dot{m} = -Q_r. \tag{13}$$

According to Refs. [25,41,42], the ablation rate in the slab target is $1.7 \times 10^{-4} \frac{I^{2/3}A^{7/6}}{(\log\Lambda)^{1/3}Z^{3/2}t^{1/3}}\ \frac{\mathrm{g}}{\mathrm{cm}^2 \cdot \mathrm{s}}$. In the conical target model, the authors carried out the following approximate treatment: the ablation rate is approximately equal to $\dot{m} = 1.7 \times 10^{-4} \frac{I^{2/3}A^{7/6}}{\theta r(\log\Lambda)^{1/3}Z^{3/2}t^{1/3}}\ \frac{\mathrm{g}}{\mathrm{cm}^2 \cdot \mathrm{s}}$. The authors consider the equation for the sound speed as $C_s^2 = ZT/M_i$, and use the ionization degree formula of the corona region: $Z = \frac{20}{3}[A(T/\mathrm{keV})]^{1/3}$, where A is the atomic number of the considered element and M_i is the proton mass.[44,45] Hence, the authors obtain the following equation:

$$1.05 \times 10^{-13} \frac{I^{2/3}A(T/\mathrm{keV})^{5/6}}{\theta r(M_i/g)(\log\Lambda)^{1/3}t^{1/3}}\ \frac{\mathrm{g}}{\mathrm{s}^3} = -Q_r. \tag{14}$$

The following equation is obtained by Eq. (14) and the electron heat flux equation $Q = -\frac{2}{7}k_0 \frac{\partial T_e^{7/2}}{\partial r}$, resulting in

$$3.86 \times 10^{-13} \frac{I^{2/3}A}{K_0\theta(M_i/g)(\log\Lambda)^{1/3}t^{1/3}} \ln(r\theta)\ \frac{\mathrm{g}}{\mathrm{s}^3 \cdot \mathrm{keV}^{5/6}} = T^{11/3} + c_1. \tag{15}$$

The authors assume the constant

$$a = 3.86 \times 10^{-13} \frac{I^{2/3}A}{K_0\theta(M_i/g)(\log\Lambda)^{1/3}t^{1/3}}\ \frac{\mathrm{g}}{\mathrm{s}^3 \cdot \mathrm{keV}^{5/6}}; \tag{16}$$

therefore, equation (15) is converted to

$$T^{8/3} = a\ln(r\theta) + c_1. \tag{17}$$

However, due to the specific properties of logarithmic functions, the authors have made a translation of the function image of Eq. (17) so that the results of interest in the specified interval can be obtained as

$$T^{8/3} = a\ln(r\theta + 1) + c_1; \tag{18}$$

at the same time, the authors focus on the boundary condition of the conduction region. When $r=0$, $T\approx T_{\rm c}$ (where $T_{\rm c}$ is the temperature of the corona region). Additionally, when $r=-L_r$, $T\approx 0$. Therefore, the solution for temperature is

$$T=T_{\rm c}\left(1-\frac{\ln(r\theta+1)}{\ln(L_r\theta+1)}\right)^{3/8}, \tag{19}$$

and since the origin of the coordinates is on the critical density surface, the value of r is considered to be in the range $[-L_r,0]$. Then, the following results are obtained using the coordinate transformation of Eq. (19):

$$T=T_{\rm c}\left(1-\frac{\ln(1-r\theta)}{\ln(L_r\theta+1)}\right)^{3/8}. \tag{20}$$

The plasma temperature solution for the corona region in the flat target has been given by Li[46,47] and can be used as a boundary for the temperature of the conduction zone in the conical target:

$$T_{\rm c}=8.34D^{1/3}I^{5/9}A^{2/9}\Lambda^{2/9}\lambda^{2/3}t^{2/9}\ \text{keV}. \tag{21}$$

According to the simulation program, $T_{\rm corona}\approx 7.8$ keV and $T_{\rm ablation}\approx 3.4$ keV.

Therefore, the adjustable coefficient $D^{1/3}\approx 0.94$ and the following results are obtained:

$$T\ (\text{keV})=\left(8.34D^{1/3}I^{5/9}A^{2/9}\Lambda^{2/9}\lambda^{2/3}t^{2/9}-3.4\right)\times\left(1-\frac{\ln(1-r\theta)}{\ln(L_r\theta+1)}\right)^{3/8}+3.4\ \text{keV}, \tag{22}$$

where the value range of $r_{(\rm cm)}$ is $[-L_r,0]$ and the value range of θ is between 90° and 120°. Equations (2) and (22) show that, when the driving laser intensity and pulse time are guaranteed to be constant, the larger the angle θ, the higher the temperature near the coronal region. Similarly, if the angle θ is held constant, increasing the intensity of the drive laser will also lead to a higher temperature near the coronal region, i.e., the temperature trend in the conduction zone will also become steeper.

Since the authors only consider the plasma length between the critical density surface (coordinate origin) and the ablation surface, based on the physical model, where $L_r=L_{r\max}$ and $T=T_{\rm c}$, the authors are interested in the length of plasma fluid from the ablation surface to the critical density surface. The approximate analytical model can be expressed as follows:

$$L_r\ (\mu\text{m})=31.5I^{1/3}\Lambda^{-1/6}t^{1/3}\theta^{-1/2}\ \mu\text{m}. \tag{23}$$

Based on the ideal state gas pressure formula $P=\rho C_{\rm s}^2$ and formula $C_{\rm s}^2\approx ZT/M_{\rm i}$, the authors obtain the approximate isobaric analytical model of the conduction region:

$$P=\rho C_{\rm s}^2=9.30Z^{-1}A^{1/3}{\rm e}^{-r/L_r}\ (T/\text{keV})^{4/3}\ \text{Mbar}, \tag{24}$$

where

$$T\ (\text{keV})=\left(8.34D^{1/3}I^{5/9}A^{2/9}\Lambda^{2/9}\lambda^{2/3}t^{2/9}-3.4\right)\times\left(1-\frac{\ln(1-r\theta)}{\ln(L_r\theta+1)}\right)^{3/8}+3.4\ \text{keV}.$$

Equation (23) and figure 4 are the relationships between the plasma length and the time in the conduction region. As can be seen from Eq. (23), when the pulse time and angle θ are guaranteed, the desired increase in plasma length can be achieved by enhancing the intensity of the driving laser. Similarly, the plasma length can also be regulated by adjusting the pulse time and angle θ when the laser intensity is determined. It can also be seen from Fig. 4 that the larger the angle θ of the conical target, the smaller the length of the plasma will be when the pulse width is certain.

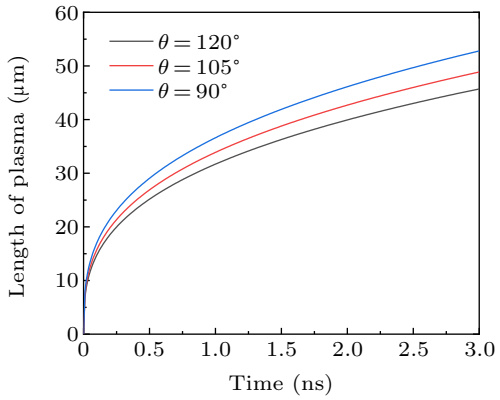


Fig. 4. Evolution of plasma length as a function of time, where $I=3.0\times 10^{14}$ W/cm^2. It can be seen that the length of the plasma increases slowly over time. Obviously, the plasma length rises faster in the first nanosecond.

According to Newton's second law and the pressure formula $P=\rho C_{\rm s}^2$, the authors obtain the following equations:

$$F=ma, \tag{25}$$

$$\frac{F}{SL_r}=\frac{ma}{SL_r}, \tag{26}$$

$$a=\frac{C_{\rm s}^2}{L_r}. \tag{27}$$

Integrating Eq. (27), the solution for the velocity is as follows:

$$v=\int a{\rm d}t=7.2\times 10^3 I^{11/27}A^{-10/27}\Lambda^{7/54}\lambda^{8/9}t^{26/27}\times\left(1-\frac{\ln(1-r\theta)}{\ln(L_r\theta+1)}\right)^{1/2}\frac{\mu\text{m}}{\text{ns}}. \tag{28}$$

3. Verification and discussion

To verify the accuracy of the analysis results, the authors compared the results in this paper with a simulation program. A single-temperature computational fluid dynamics program based on Euler's equation was utilized,[48] and the control equation is as follows:

$$\frac{\partial\rho}{\partial t}+\frac{1}{r^2}\frac{\partial(\rho r^2V_r)}{\partial r}=0, \tag{29}$$

$$\frac{\partial(\rho V_r)}{\partial t}+\frac{1}{r^2}\frac{\partial(\rho V_r^2 r^2)}{\partial r}=(\nabla\cdot P)_r, \tag{30}$$

$$\frac{\partial(\rho e)}{\partial t}+\frac{1}{r^2}\frac{\partial}{\partial r}(\rho e r^2 V_r)$$
$$=-\frac{P}{r^2}\frac{\partial}{\partial r}(r^2 V_r)+\frac{1}{r^2}\frac{\partial}{\partial r}\left(K_e r^2\frac{\partial T}{\partial r}\right)+S. \tag{31}$$

where ρ, V_r, e, T, and P represent the density, velocity, total energy, temperature, and pressure, respectively. S is the laser energy deposition term induced by inverse bremsstrahlung absorption. The Spitzer–Harm model[49] was used for the electron heat transfer, and K_e is the heat transfer coefficient. The finite volume method (FVM) was used for the fluid solution, with a non-uniform sparse grid being set at locations away from the target to extend the computational domain. Moreover, a dynamic grid function was added to ensure that the flow field remains in the encrypted grid. To compare the analytical results, the above equation is solved in a spherical coordinate system, and a one-dimensional laser shot problem is calculated taking into account the shrinkage effect.

The same conditions were set for the simulation and analysis model: driving laser power density $I=3.0\times10^{14}$ W/cm^2, wavelength $\lambda=0.351$ μm, and pulse width $t=1.0$ ns. The comparison between the analysis results and the program simulation results is shown in Fig. 5, which includes the plasma density, temperature, pressure, and velocity in the conduction region of the conical target.

It is obvious from Fig. 5 that the analytical model developed in this paper and the numerical simulation results are generally consistent, although they show a small deviation in terms of values. This can be explained and their trends are consistent. In the model of this paper, when the laser is incident from the right, it can be seen that the left side of the conduction region is the compression zone. Therefore, the authors assume that the ablation surface also has a width, which leads to the fact that the plasma density at the ablation surface is unequal to the density of the solid fuel (Fig. 5(a)).

In the analytical process, the temperature of the ablation surface is approximated as 0 keV for computational convenience. However, in Fig. 5(b), the authors combine the data given by the simulation results and compare the trend with the temperature simulation results, and find that they are in general agreement with each other. In the conduction region, the plasma temperature increases quickly initially and then slowly with the passage of time, and the authors approximate that the plasma temperature remains constant in the coronal region.

In Fig. 5(c), the analytical results of the pressure and the simulation are in general agreement. In fact, the pressure decreases gradually and slowly from the ablation surface to the critical density surface, which can also be seen in the figure, but in the analysis, the authors approximate that it is an isobaric process, i.e., the pressure remains essentially constant.

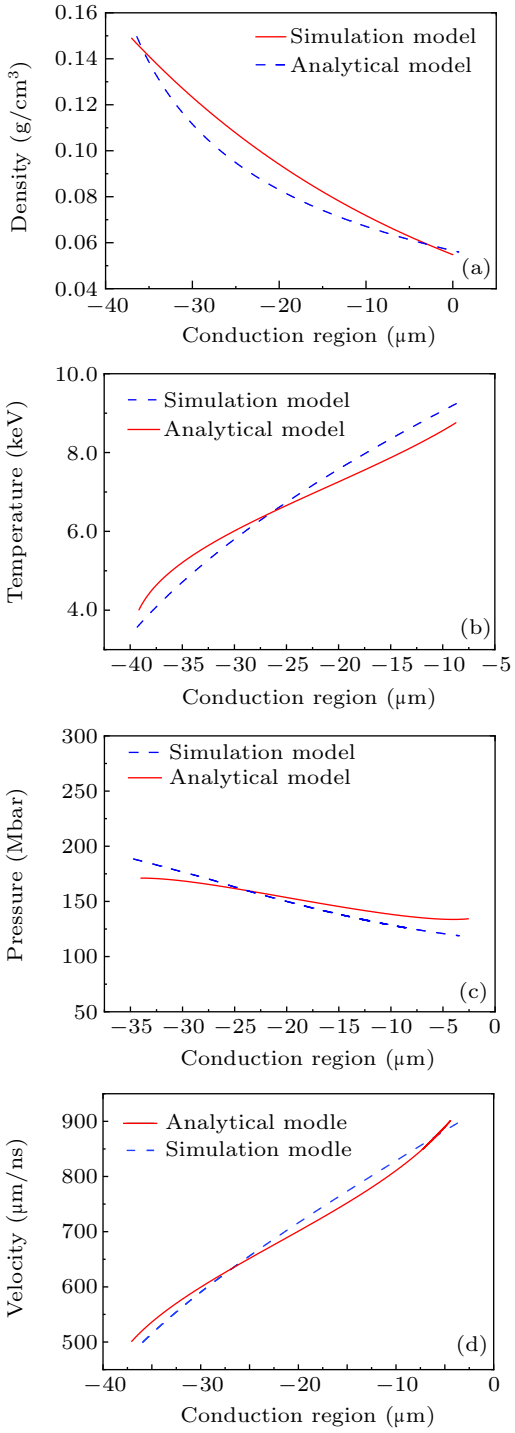


Fig. 5. Density (a), temperature (b), pressure (c), and velocity (d) in the conduction region. It is noteworthy that the authors take the critical density surface as the coordinate origin.

In the density model given in Eq. (12), adjusting the laser light intensity and pulse duration led to a change in the density gradient (Figs. 3 and 6), i.e., increasing the former two parameters reduces the gradient, but the effect is insignificant for the suppression of γ. In other words, this adjustment in the proposed model has almost no effect on the Atwood number in Eq. (1). Therefore, the authors focus on the effect of the plasma length model on the RTI growth rate.

The ablation velocity V_a in Eq. (1) can be treated as a constant.[50] According to the model in this paper, the linear

growth curves γ influenced by wavelength λ and the length of the plasma in the conduction zone are shown in Fig. 7.

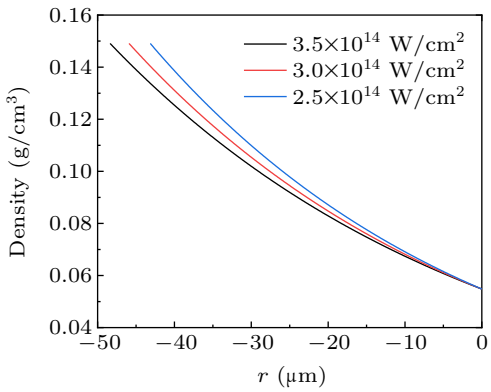


Fig. 6. Density curves at different laser intensities. The pulse width $t = 1.0$ ns.

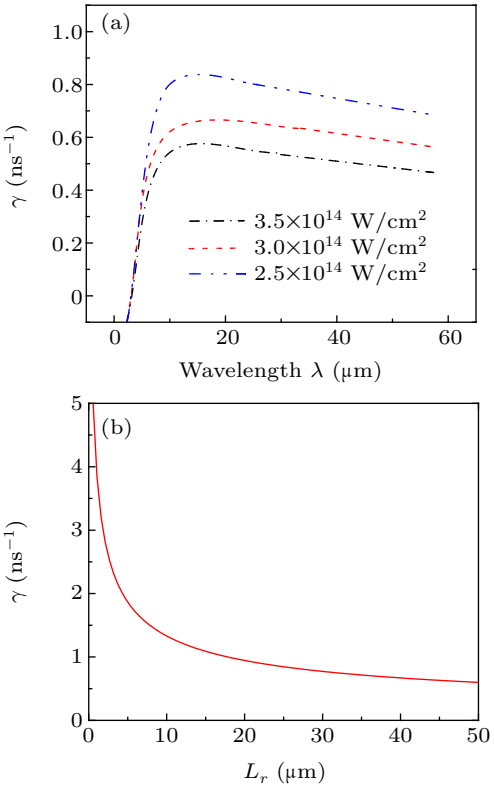


Fig. 7. Linear growth curves γ influenced by wavelength λ (a) and L_r (b). For the selection of acceleration g, the authors refer to the values in the numerical simulation of ablation RTI by Ye *et al.*,[51] where $g = 17.85$ μm/ns^2 . Atwood number $A \approx 0.5$, and according to the model in this paper, $\rho_1 \approx 0.054$ g/cm^3 and $\rho_2 \approx 0.158$ g/cm^3. In (b), the perturbation wave number $k = 2\pi/\lambda$ and $\lambda = 0.351$ μm.

Overall, γ decays as L_r increases; however, which of the two, laser intensity or pulse time width, has a more significant effect on the growth rate γ will be discussed here (Fig. 8).

Figure 8 shows that increasing the laser intensity and pulse duration or decreasing the angle θ as appropriate can attenuate the RTI growth rate. It is worth noting that adjusting the laser pulse duration is more beneficial for attenuating the RTI growth rate, and changing the laser intensity has a limited impact on γ. The change in angle θ also has an effect on γ, but it is negligible. In order to observe more clearly the effect of the change in laser intensity on γ, the growth rate curve γ influenced by laser intensity is shown here separately (Fig. 9).

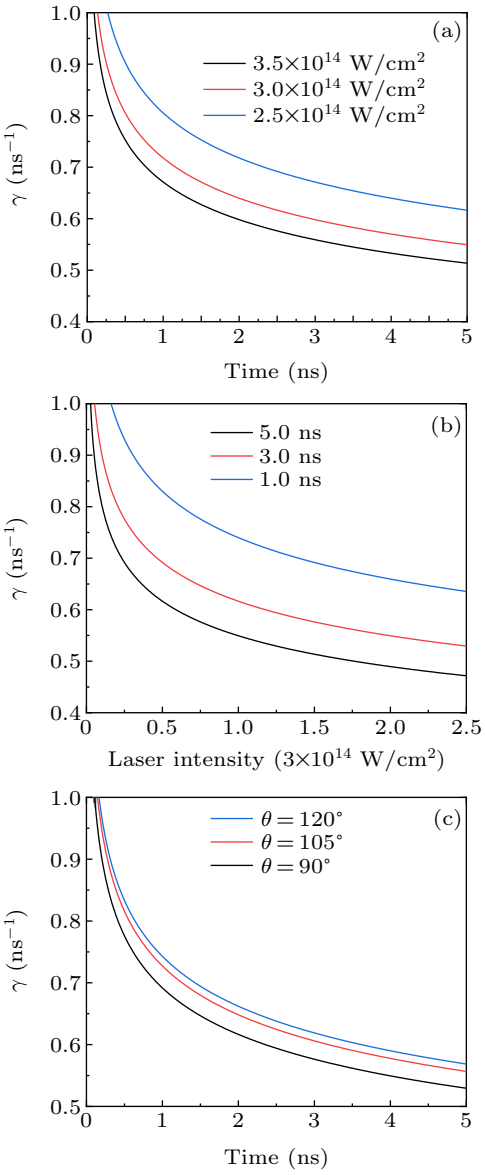


Fig. 8. Linear growth curves γ influenced by laser intensity (a), time (b), and angle θ of the conical target (c). In (a) and (b), the angle θ of the conical target is chosen to be 90°, and in (c), driving laser power density $I = 3.0 \times 10^{14}$ W/cm^2.

When the laser intensity is adjusted around $I = 3.0 \times 10^{14}$ W/cm^2 in the experiment, the change in the growth rate γ is minimal (Fig. 9). There is only a fractional change in the order of magnitude. Moreover, it is necessary to drastically change the laser intensity to suppress the growth rate, but it is much easier and more efficient to alter the pulse duration.

Analytical solutions for the density, temperature, and length of the plasma are shown in Eqs. (12), (22), and (23), which are key works of this paper. Here the effect of the parameters in the proposed model on the RTI of the ablation surface is explicitly analyzed, emphasizing the significance of RTI analysis to the work in this paper. As the plasma length grows, the RTI caused by the density gradient is attenuated.

When the angle of the conical target is 90°, appropriately increasing the pulse duration or increasing the laser intensity is beneficial to suppressing the growth rate γ. However, adjusting the pulse duration will be more efficient than changing the laser intensity.

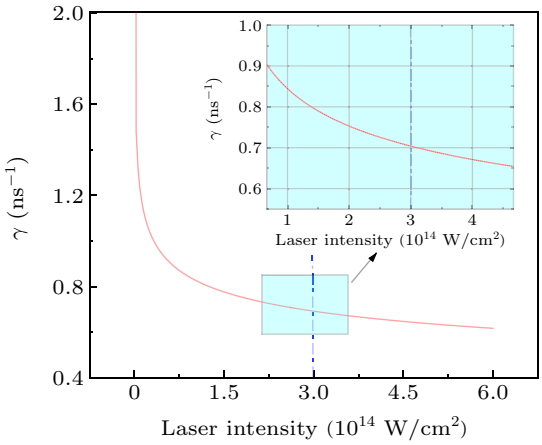


Fig. 9. Partial enlargement of the growth rate curve γ. The baseline for the laser intensity is chosen here as $I = 3.0 \times 10^{14}$ W/cm^2, pulse width $t = 1.0$ ns, and angle $\theta = 90°$.

4. Summary

In summary, an isobaric, steady-state model of a plasma fluid in the conduction zone is provided in this work to discuss and resolve the RTI present in the double-cone ignition scheme. Within the angle range of the conical target (90°–120°), the pulse width and laser intensity are appropriately increased when the angle is 90° , which is the most favorable for attenuating the RTI on the ablation surface, and increasing the pulse duration is more efficient than increasing the laser intensity and adjusting the angle (Fig. 7). Notably, the study of the hydrodynamics of the plasma in the conical target conduction region using analytical methods has not been proposed at all in previous works.

Equations (12) and (23) show that laser intensity and time also affect the density trend in the conduction zone: increasing the laser intensity and pulse duration leads to a smaller density gradient and a longer length L of the plasma. The temperature solution of the energy equation of the fluid dynamics model is shown in Eq. (22). Increasing the laser intensity and time also increases the temperature near the critical density surface, which can have an impact on the temperature trend in the conduction zone. The two-dimensional calibration relations for the length, pressure, and velocity models of the plasma fluid in the conduction zone are provided by Eqs. (23), (24), and (28). The adjustable parameters in L_r provide convenience for the analysis of RTI on the ablation surface in the conical target. It can be concluded that extending the pulse duration is a more practical approach than increasing the laser intensity. Clearly, compared with the numerical simulation of two-dimensional fluid mechanics, the method proposed in this paper provides theoretical methods and mechanisms instead of only numerical solutions. The isobaric steady-state analytical model in the conduction region established in this paper demonstrates clear physical images and robust results, which are useful for analyzing the favorable conditions for attenuating RTI in a conical target.

Acknowledgment

Project supported by the Strategic Priority Research Program of Chinese Academy of Sciences (Grant Nos. XDA 25051000 and XDA 25010100).

References

[1] Betti R and Hurricane O A 2016 *Nat. Phys.* **12** 435
[2] Frenje J A 2020 *Plasma Phys. Control. Fusion* **62** 023001
[3] Zhang S and Hu S X 2020 *Phys. Rev. Lett.* **125** 105001
[4] Betti R, Goncharov V N, McCrory R L and Verdon C P 1998 *Phys. Plasmas* **5** 1446
[5] Henderson D B, McCrory R L and Morse R L 1974 *Phys. Rev. Lett.* **33** 205
[6] Yang H, Zhang J and Li Y 2002 *Phys. Rev. E* **66** 016406
[7] Colaïtis A, Duchateau G and Ribeyre X 2015 *Phys. Rev. E* **92** 041101
[8] Hill D W and Kingham R J 2018 *Phys. Rev. E* **98** 021201
[9] Clark T R and Milchberg H M 1998 *Phys. Rev. E* **57** 3417
[10] Duchateau G, Hu S X and Pineau A 2019 *Phys. Rev. E* **100** 033201
[11] Lindl J D, Amendt P and Berger R L 2004 *Phys. Plasmas* **11** 339
[12] Lindl J 1995 *Phys. Plasmas* **2** 3933
[13] Perkins L J, Betti R and LaFortune K N 2009 *Phys. Rev. Lett.* **103** 045004
[14] Marozas J A, Hohenberger M and Rosenberg M J 2018 *Phys. Rev. Lett.* **120** 085001
[15] Livescu D, Wei T and Petersen M R 2011 *J. Phys.: Conf. Ser.* **318** 082007
[16] Livescu D, Ristorcelli J R and Gore R A 2010 *Phys. Scr.* **T142** 014015
[17] Livescu D 2004 *Phys. Fluids* **16** 118
[18] Yu X J, Ye W H and Wu J F 2006 *High Power Laser Particle Beams* **08** 1297
[19] Gupta N K and Lawand S V 1986 *Plasma Phys. Control. Fusion* **28** 925
[20] Sanz J 1996 *Phys. Rev. E* **53** 4026
[21] Zhang J, Wang W M and Yang X H 2020 *Phil. Trans. R. Soc. A* **378** 20200015
[22] Sanz J, Masse L and Clavin P 2006 *Phys. Plasmas* **13** 102702
[23] Guo H Y, Cheng T, Li J and Li Y J 2022 *Chin. Phys. B* **31** 35203
[24] Fang K, Zhang Z and Li Y T 2022 *Acta Phys. Sin.* **71** 035204 (in Chinese)
[25] De Groot J S, Estabrook K G, Kruer W L, Drake R P, Mizuno K, and Cameron S M 1992 *Physics of Fluids B: Plasma Physics* **4** 701
[26] Li Y J, Zhang G P and Zhang J 1999 *Chinese Journal of Computational Physics* **05** 529
[27] Zeng X C, Jiang R H and Chang T Q 1991 *High Power Laser and Particle Beams* **04** 477
[28] Zhang J, Pei W B, Gu P J and Chang T Q 1995 *Acta Phys. Sin.* **44** 1936 (in Chinese)
[29] Christopherson A R, Betti R and Lindl J D 2019 *Phys. Rev. E* **99** 021201
[30] Ye W H, Zhang W Y and He X T 2000 *Acta Phys. Sin.* **49** 0762 (in Chinese)
[31] Li J and Zhao 2010 *Plasma Phys. Control. Fusion* **52** 045013
[32] Grun J, Decoste R, Ripin B H, *et al.* 1998 *Appl. Phys. Lett.* **39** 545
[33] Zhang J, Zhang Z and Wang W M (CN Patent) 111681783 A [2020-09-18]
[34] Betti R, Goncharov V N and McCrory R L 1981 *Phys. Plasmas* **5** 1446
[35] Kilkenny J D, Glendinning S G and Haan S W 1994 *Phys. Plasmas* **1** 1379
[36] Tabak M, Munro D H and Lindl J D 1990 *Phys. Plasmas* **2** 1007
[37] London R A and Rosen M D 1986 *Phys. Fluids* **29** 3813
[38] Sanz J, Garnier J and Cherfils C 2005 *Phys. Plasmas* **12** 112702
[39] Yabe T, Mima K and Yoshikawa K 1981 *Nucl. Fusion* **21** 803

[40] Chang T Q 1991 *Laser Plasma Interaction and Laser Fusion* (Hunan: Hunan Science and Technology Press) p. 185
[41] Lobok M G, Andriyash I A and Vais O E 2021 *Phys. Rev. E* **104** L053201
[42] De Groot J S, Cameron S M and Mizuno K 1991 *Phys. Plasmas* **3** 1241
[43] Fabbro R, Max C and Fabre E 1985 *Phys. Fluids* **28** 1463
[44] Colombant D and Tonon G F 1973 *J. Appl. Phys.* **44** 3524
[45] Bobin J L, Colombant D and Tonon G 1972 *Nucl. Fusion* **12** 445
[46] Li Y J and Zhang J 2001 *Phys. Rev. E* **63** 036410
[47] Li Y J, Lu X and Zhang J 2002 *Phys. Rev. E* **66** 046501
[48] Li Z Y, Wang L F, Wu J F and Ye W H 2020 *Chin. Phys. B* **29** 034704
[49] Spitzer L and Harm R 1952 *Phys. Rev.* **89** 977
[50] Ye W H, Zhang W Y and He X T 2002 *Phys. Rev. E* **65** 057401
[51] Ye W H, Wang L F and He X T 2010 *Phys. Plasmas* **17** 122704